Pressure-induced phase transitions in single-crystalline $Cu_4Bi_4S_9$ nanoribbons*

Hu Jing-Yu(胡靖宇)[a)b)], Li Jing(李 劲)[a)], Zhang Si-Jia(张思佳)[b)], Zhao Hao-Fei(赵豪飞)[b)], Zhang Qing-Hua(张庆华)[b)], Yao Yuan(姚 湲)[b)], Zhao Qing(赵 清)[a)], Shi Li-Jie(石丽洁)[a)], Zou Bing-Suo(邹炳锁)[a)], Li Yan-Chun(李延春)[c)], Li Xiao-Dong(李晓东)[c)], Liu Jing(刘 景)[c)], Zhu Ke(朱 恪)[b)], Liu Yu-Long(刘玉龙)[b)], Jin Chang-Qing(靳常青)[b)], and Yu Ri-Cheng(禹日成)[b)†]

[a)] *School of Physics, Beijing Institute of Technology, Beijing* 100081, *China*

[b)] *Beijing National Laboratory for Condensed Matter Physics, Institute of Physics, Chinese Academy of Sciences, Beijing* 100190, *China*

[c)] *Institute of High Energy Physics, Chinese Academy of Sciences, Beijing* 100039, *China*

(Received 13 May 2013; revised manuscript received 8 June 2013)

In situ angle dispersive synchrotron X-ray diffraction and Raman scattering measurements under pressure are employed to study the structural evolution of $Cu_4Bi_4S_9$ nanoribbons, which are fabricated by using a facile solvothermal method. Both experiments show that a structural phase transition occurs near 14.5 GPa, and there is a pressure-induced reversible amorphization at about 25.6 GPa. The electrical transport property of a single $Cu_4Bi_4S_9$ nanoribbon under different pressures is also investigated.

Keywords: $Cu_4Bi_4S_9$ nanoribbon, high pressure, amorphization, phase transition

PACS: 62.50.–p, 61.05.cp, 78.30.–j, 64.70.K– **DOI:** 10.1088/1674-1056/22/11/116201

1. Introduction

Copper-based multi-component chalcogenides (CBMC) have been widely investigated in recent years for their potential applications as advanced materials and energy-harvesting devices in solar cells. Recently, nanoscale solar cells have been recognized as a promising class of photovoltaic devices because their nanoscale dimension permits a large amount of free movement and more efficient collection of electrons,[1] so the CBMC with nano (micro) structures has received increased interest. For example, Ward *et al.*[2] reported that the efficiency of the $CuIn_xGa_{1-x}Se_2$ system as a polycrystalline thin-film solar cell could exceed 20%. Paire *et al.*[3] found that the microscale solar cells of $CuIn_xGa_{1-x}Se_2$ could improve the absolute efficiency by 4% because the microcell structure leads to a strong decrease in resistive losses.

Since the Cu–Bi–S compounds consist of the earth-abundant and inexpensive elements of Bi and S, they become key members of the CBMC family. Nair *et al.*[4] reported the fabrication of the Cu_3BiS_3 compound and indicated that it may be applied in solar cells. Later, Gerein *et al.*[5] improved the synthesis of Cu_3BiS_3 thin film and measured its optical and electrical properties. They found that the Cu_3BiS_3 film could be a useful light absorber layer in solar cells due to its narrow band gap, high optical absorption coefficient, and good electrical conductivity. In 2011, Li *et al.*[6] fabricated single-crystalline $Cu_4Bi_4S_9$ nanoribbons by using a facile solvothermal method and investigated their optical properties. The results showed that the $Cu_4Bi_4S_9$ nanoribbons enhance the surface photovoltage response in the whole visible wavelength range, and their photoinduced charge (electron–hole pairs) separation efficiency in the visible-light region is higher than that in the near-infrared.[6] These properties mean that $Cu_4Bi_4S_9$ nanoribbons could potentially be used in optoelectronic devices such as solar cells. As nanoribbons can be the building blocks of nano devices, it is essential to study the electronic properties of an individual nanoribbon for the design and optimization of nano devices. The electrical transport properties of a single $Cu_4Bi_4S_9$ nanoribbon could provide useful information for its potential applications.

As is well known, the structure of a material determines its physical properties. A high pressure can tune the crystal and electronic structures of a material and further affect its electrical and optical properties, which are closely related to the photovoltaic applications.[7,8] Recently, the investigation on the high pressure phases of materials has been further extended to nanomaterials.[9–11] In this work, we investigate the structural stability of $Cu_4Bi_4S_9$ nanoribbons under pressure through *in situ* high pressure angle dispersive synchrotron X-ray diffraction (AD-XRD) experiments and Raman scattering measurements, and study the electrical transport property of a single $Cu_4Bi_4S_9$ nanoribbon.

*Project supported by the National Basic Research Program of China (Grant No. 2012CB932302) and the National Natural Science Foundation of China (Grant No. 11174336).

†Corresponding author. E-mail: rcyu@aphy.iphy.ac.cn

© 2013 Chinese Physical Society and IOP Publishing Ltd

2. Experimental details

Single-crystalline $Cu_4Bi_4S_9$ nanoribbons were fabricated by using a facile solvothermal method, the preparation details have been reported elsewhere.[6] The size and morphology of the samples were determined by using a Hitachi Model S-4800 field-emission scanning electron microscope (SEM). *In situ* high pressure AD-XRD measurements up to about 40.4 GPa were performed at the Beijing Synchrotron Radiation Facility at room temperature. The X-ray wavelength was 0.06199 nm and the diffracted X-ray was detected with an imaging plate. The high pressure was generated by using a symmetric type diamond-anvil cell (DAC) with 300 μm culets. The sample was loaded into the sample chamber in a T301 stainless steel gasket, and the pressure was measured by using the ruby fluorescence technique.[12] *In situ* high pressure Raman scattering measurements up to about 25.6 GPa were carried out with a LABRAM-HR confocal laser micro-Raman spectrometer (HR800), also using the DAC technique. The 532 nm line of a Verdi-2 solid-state laser was used as the Raman excitation source. A 25× microscope objective lens was used to focus the laser beam and collect the scattered light. Because the intensities of the reflection of the $Cu_4Bi_4S_9$ nanoribbons were very weak, we did not use any pressure transmitting medium in our experiments. Normally, a pressured induced phase transition occurs at a lower pressure in non-hydrostatic compression as compared with that in hydrostatic compression. In addition, the peak width would be broadened under the non-hydrostatic condition due to the pressure gradient in the sample.

The focused ion beam (FIB) technique was employed to weld electrodes for the measurements of the temperature dependence of electrical resistivity of a single $Cu_4Bi_4S_9$ nanoribbon. The $Cu_4Bi_4S_9$ nanoribbons were spread on a silicon oxide surface and an appropriately isolated one was identified by using the SEM. Then two pairs of Pt microleads typically 500 nm in width and 100 nm in thickness were fabricated by FIB deposition. Finally, the electrical connection between the Pt microleads and the sample holder was made using highly conductive silver paste and Pt wires. The measurements of temperature-dependent resistance $R(T)$ under hydrostatic pressures up to 2.4 GPa were carried out by using the four-probe technique in a pistoncylinder pressure cell, with a 1:1 mixture of silicon oil and coal oil as the pressure transmitting medium.

3. Results and discussion

A typical morphologic image of the $Cu_4Bi_4S_9$ nanoribbons is shown in Fig. 1. The ribbon-like structure is clearly revealed. The widths of the sample are mostly in the range from 30 nm to 100 nm, and the lengths can exceed several micrometers. It was reported that the $Cu_4Bi_4S_9$ nanoribbon shows an orthorhombic structure with space group *Panm* and its cell parameters are $a = 31.528$ Å, $b = 11.622$ Å, $c = 3.951$ Å.[6] As shown in Fig. 2, all the diffraction peaks of the AD-XRD pattern at 0.03 GPa can be indexed on the basis of the JCPDS file card No. 77-1238. It is consistent with the earlier report.[6] Compared with the peaks in the JCPDS card, the intensities of a few peaks are reversed, for example (031) and (131), this may be due to the preferred orientation of the nanoribbons under pressure.



Fig. 1. SEM image of single-crystalline $Cu_4Bi_4S_9$ nanoribbons.

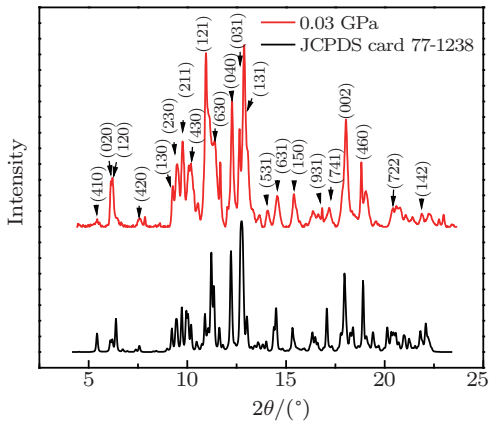


Fig. 2. (color online) AD-XRD pattern of the $Cu_4Bi_4S_9$ nanoribbons at 0.03 GPa.

The AD-XRD patterns of the $Cu_4Bi_4S_9$ nanoribbons at different pressures are shown in Fig. 3. In the pressure range from 0.03 GPa to 9.17 GPa, the diffraction peaks become broader and weaker and gradually shift to larger angles with increasing pressure, this shows the compression of the lattice. From 9.17 GPa to 14.5 GPa, some peaks begin to shift towards smaller angles with increasing pressure (indicted by $*$), it indicates that the crystal structure of the $Cu_4Bi_4S_9$ nanoribbons starts to change. When the pressure reaches 14.5 GPa, a new peak appears (indicted by a ♦), it means that the pressure induces a new structural phase in the $Cu_4Bi_4S_9$ nanoribbons. Above 14.5 GPa, the diffraction peaks shift to larger angles again with increasing pressure. All other peaks, except the peak of the new phase, vanish at 26.9 GPa, and some broad

bands occur; this indicates that the structure of the $Cu_4Bi_4S_9$ nanoribbons partly transforms into an amorphous structure. With increasing pressure from 31.4 GPa up to 40.4 GPa, the diffraction pattern stays similar, it indicates that the structure of the $Cu_4Bi_4S_9$ nanoribbons under high pressure is the coexistence of the new phase and amorphization. When the pressure is released to ambient pressure, some original peaks are recovered; this indicates that the amorphization of the $Cu_4Bi_4S_9$ nanoribbons is reversible.

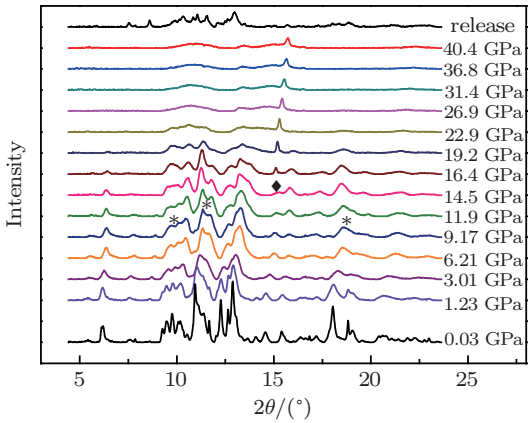


Fig. 3. (color online) AD-XRD patterns of the $Cu_4Bi_4S_9$ nanoribbons at different pressures.

From *in situ* high pressure AD-XRD measurements, we find that the structure of the $Cu_4Bi_4S_9$ nanoribbons transforms to a new phase at 14.5 GPa. Because only one peak of the new phase appears in the measured patterns, we are not able to identify the structure of this new phase. At least, the results suggest that the new phase has a crystal structure with a higher symmetry.

The pressure dependences of relative shrinkage of the lattice parameters of the orthorhombic $Cu_4Bi_4S_9$ nanoribbons are shown in Fig. 4(a). With increasing pressure, a/a_0, b/b_0, and c/c_0 decrease. The decreasing rate of a/a_0 is smaller than that of b/b_0 and c/c_0 below 3 GPa, while it is larger above 3 GPa. This result indicates that the compression of the crystal lattice exhibits an anisotropic characteristic. Figure 4(b) shows the relative volume V/V_0 (normalized to the zero pressure volume) of the orthorhombic $Cu_4Bi_4S_9$ nanoribbons as a function of pressure, where the solid line is the fitting result using the Birch–Murnaghan equation

$$P = \frac{3}{2}B_0\left[\left(\frac{V}{V_0}\right)^{-7/3} - \left(\frac{V}{V_0}\right)^{-5/3}\right] \times\left\{1-\frac{3}{4}(4-B_0')\left[\left(\frac{V}{V_0}\right)^{-2/3}-1\right]\right\}. \quad (1)$$

With the pressure derivative B_0' fixed at 4, we obtain the bulk modulus $B_0 = 90.9$ GPa. Compared with other CMBC materials, the bulk modulus of the orthorhombic $Cu_4Bi_4S_9$ nanoribbons is just between the chalcopyrite phase (75 GPa) and the cubic phase (123 GPa) of $CuInS_2$.[13]

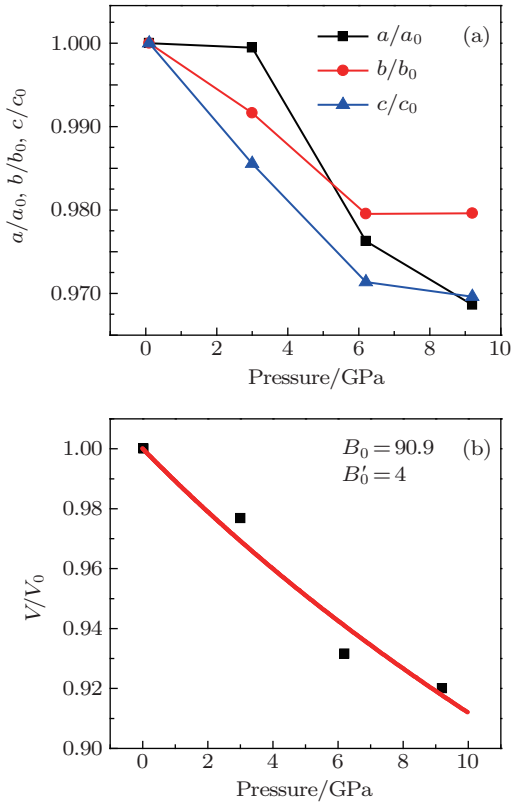


Fig. 4. (color online) (a) The pressure dependence of relative shrinkage of the lattice parameters of the orthorhombic $Cu_4Bi_4S_9$ nanoribbons, (b) the relative volume V/V_0 as a function of pressure. The solid line in panel (b) is the fitting result with the Birch–Murnaghan equation of state.

In order to further confirm the pressure induced phase transitions in the $Cu_4Bi_4S_9$ nanoribbons, we performed *in situ* high pressure Raman scattering measurements. In Fig. 5, we display the Raman scattering spectra at different pressures up to 25.6 GPa at room temperature in the frequency region 200–1100 cm^{-1}. As shown in Fig. 5, the Raman spectrum of the $Cu_4Bi_4S_9$ nanoribbons at 0.4 GPa contains seven different Raman active modes: 255 cm^{-1}, 300 cm^{-1}, 318 cm^{-1}, 443 cm^{-1}, 475 cm^{-1}, 939 cm^{-1}, and 986 cm^{-1}. With increasing pressure, all the peaks shift towards higher frequencies, and the intensities of the peaks at 255 cm^{-1}, 300 cm^{-1}, 318 cm^{-1}, 443 cm^{-1}, 475 cm^{-1} become weaker. When the pressure reaches 5.4 GPa, three peaks (255 cm^{-1}, 318 cm^{-1}, 443 cm^{-1}) become indiscernible. Then the peak at 300 cm^{-1} disappears at 8.8 GPa. At 12.5 GPa, which is just below the phase transition pressure of 14.5 GPa obtained from AD-XRD, two new Raman active modes appear at 472 cm^{-1} and 1032 cm^{-1} (indicated by ♦), indicating that the structure of the $Cu_4Bi_4S_9$ nanoribbons has changed. As the pressure increases to 25.6 GPa, all peaks except the new Raman peaks are invisible and the Raman spectrum becomes broad bands; it indicates the partial amorphization of the sample. When the pressure releases to ambient pressure, some original Raman active modes reappear. This means that the amorphization of the $Cu_4Bi_4S_9$ nanoribbons is reversible. These results are consistent with the

phase transitions observed in our AD-XRD experiments.

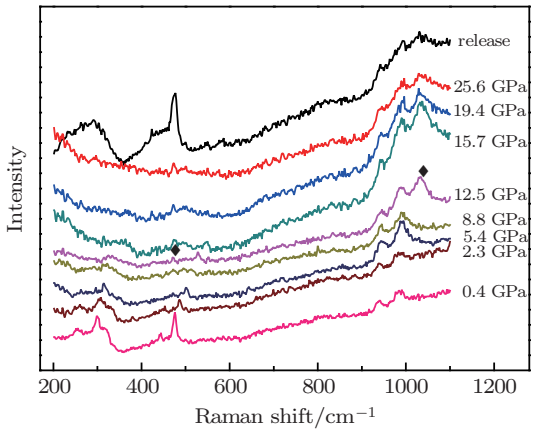


Fig. 5. (color online) Raman spectra of the $Cu_4Bi_4S_9$ nanoribbons at different pressures.

The temperature dependences of the electrical resistivity for a single $Cu_4Bi_4S_9$ nanoribbon under different pressures are shown in Fig. 6(a). The electrical resistivity increases quickly with decreasing temperature, indicating that the $Cu_4Bi_4S_9$ nanoribbon is a semiconductor. With increasing pressure up to 2.4 GPa, the transport behaviors are similar. It means that such low pressures cannot cause any apparent change in the transport property. As expected, the resistivity decreases with the applied pressure from 0 to 2.4 GPa in the whole measured temperature range. Li *et al.*[14] reported that the $Cu_4Bi_4S_9$ nanowire shows two electronic transport behaviors in different temperature ranges: a typical semiconductor behavior in 10–140 K and a metal-like characteristic in 150–300 K, which is different from our results. This difference could come from two aspects. One is that the different morphologies between $Cu_4Bi_4S_9$ nanowires and $Cu_4Bi_4S_9$ nanoribbons could affect the transport property. The other is that although the $Cu_4Bi_4S_9$ nanowire and the $Cu_4Bi_4S_9$ nanoribbon have the same crystal structure, their microstructures could be different, as Li *et al.* believed that the metal-like characteristic is resulted from the phonon scattering when a lot of defects exist on the surface of the nanowire.

The thermally activated conductivity of $Cu_4Bi_4S_9$ nanoribbons can be written as

$$\sigma = \sigma_0 \exp(-E/K_B T), \tag{2}$$

where σ is the conductivity of the $Cu_4Bi_4S_9$ nanoribbon, σ_0 is the conductivity prefactor, K_B is the Boltzmann constant, T is the absolute temperature, and E is the activation energy (half the band gap). The activation energy of the carriers' motion can be estimated from $(\ln \sigma^{-1})$ versus $(1/T)$. Through fitting the temperature dependence of the resistance curve, we can obtain the activation energy of the $Cu_4Bi_4S_9$ nanoribbon as 0.761 eV above 270 K at ambient pressure. The pressure dependence of the activation energy is presented in Fig. 6(b). With increasing pressure, the activation energy of the $Cu_4Bi_4S_9$ nanoribbon decreases, which is consistent with the increase of the electrical conductivity. Similar results were also reported in the literature.[15,16] As the pressure increases to 2.4 GPa, the activation energy slightly decreases to 0.723 eV, which is 0.038 eV (5%) lower than that at ambient pressure. As the activation energy is related to the band gap, our results would be useful for the potential application of $Cu_4Bi_4S_9$ nanoribbons in photoelectric devices.

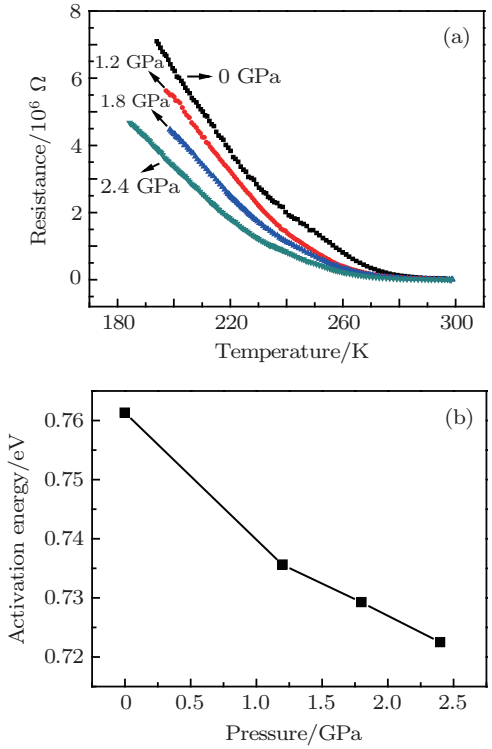


Fig. 6. (color online) (a) Temperature-dependent resistance of a single $Cu_4Bi_4S_9$ nanoribbon measured under different pressures, (b) pressure dependence of activation energies.

4. Conclusion

We fabricated single-crystalline $Cu_4Bi_4S_9$ nanoribbons by using a facile solvothermal method, and carried out *in situ* AD-XRD and Raman scattering measurements under various pressures to study the structural evolution of the $Cu_4Bi_4S_9$ nanoribbons. Pressure induced phase transition and amorphization were observed in both experiments. When the pressure released to ambient pressure, both experiments showed that the amorphization is reversible. The calculated activation energy obtained by fitting the temperature dependences of the electrical resistivity (above 270 K) at ambient pressure is 0.761 eV, and we found that the activation energy of the $Cu_4Bi_4S_9$ nanoribbon decreases with increasing pressure.

References

[1] Bierman M J and Jin S 2009 *Energy Environ. Sci.* **2** 1050
[2] Ward J S, Ramanathan K, Hasoon F S, Coutts T J, Keane J, Contreras M A, Moriarty T and Noufi R 2002 *Prog. Photovoltaics* **10** 41

[3] Paire M, Lombez L, Pere-Laperne N, Collin S, Pelouard J L, Lincot D and Guillemoles J F 2011 *Appl. Phys. Lett.* **98** 264102
[4] Nair P K, Huang L, Nair M T S, Hu H L, Meyers E A and Zingaro R A 1997 *J. Mater. Res.* **12** 651
[5] Gerein N J and Haber J A 2006 *Chem. Mater.* **18** 6297
[6] Li H X, Zhang Q L, Pan A L, Wang Y G, Zou B S and Fan H 2011 *J. Chem. Mater.* **23** 1299
[7] Gonzalez J and Rincon C 1989 *J. Appl. Phys.* **65** 2031
[8] Bovornratanaraks T, Saengsuwan V, Yoodee K, McMahon M I, Hejny C and Ruffolo D 2010 *J. Phys.: Condens. Matter* **22** 355801
[9] Yao L D, Luo S D, Shen X, You S J, Yang L X, Zhang S J, Jiang S, Li Y C, Liu J, Zhu K, Liu Y L, Zhou W Y, Chen L C, Jin C Q and Yu R C 2010 *J. Mater. Res.* **25** 2330
[10] Hu J Y, Liang S C, Piao G Z, Zhang S J, Zhang Q H, Yang Y, Zhao Q, Zhu K, Liu Y L, Tang L Y, Li Y C, Liu J, Jin C Q and Yu R C 2011 *J. Appl. Phys.* **110** 014301
[11] Shen X, Shen J, You S J, Yang L X, Tang L Y, Li Y C, Liu J, Yang H, Zhu K, Liu Y L, Zhou W Y, Jin C Q and Yu R C 2009 *J. Appl. Phys.* **106** 113523
[12] Mao H K, Xu J and Bell P M 1986 *J. Geophys. Res.* **91** 4673
[13] Tinoco T, Pollian A, Gomez D and Itie J P 1996 *Phys. Status Solidi b* **198** 433
[14] Li J, Zhong H Z, Liu H J, Zhai T Y, Wang X, Liao M Y, Bando Y, Liu R B and Zou B S 2012 *J. Mater. Chem.* **22** 17813
[15] Yao M G, Wagberg T and Sundqvist B 2010 *Phys. Rev. B* **81** 155441
[16] Parthasarathy G 2011 *Am. Mineral.* **96** 860